Available online at www.sciencedirect.com

ScienceDirect

Advances in Space Research 53 (2014) 734–743

ADVANCES IN SPACE RESEARCH (a COSPAR publication)

www.elsevier.com/locate/asr

Climatology of ionospheric scintillations and TEC trend over the Ugandan region

Emirant Bertillas Amabayo [a,b,*], Jurua Edward [a,1], Pierre J. Cilliers [c,2], John Bosco Habarulema [c,d,2]

[a] Department of Physics, Mbarara University of Science and Technology, Mbarara, Uganda
[b] Department of Physics, Busitema University, Tororo, Uganda
[c] South African National Space Agency (SANSA) Space Science, P O Box 32, Hermanus 7200, South Africa
[d] Department of Physics and Electronics, Rhodes University, 6140 Grahamstown, South Africa

Received 7 September 2013; received in revised form 9 December 2013; accepted 13 December 2013
Available online 24 December 2013

Abstract

This study presents results on the investigation of the diurnal, monthly and seasonal variability of Total Electron Content (TEC), phase (σ_Φ) and amplitude (S4) scintillation indices over Ugandan (Low latitude) region. Scintillation Network Decision Aid (SCINDA) data was obtained from Makerere (0.34°N, 32.57°E) station, Uganda for two years (2011 and 2012). Data from two dual frequency GPS receivers at Mbarara (0.60°S, 30.74°E) and Entebbe (0.04°N, 32.44°E) was used to study TEC climatology during the same period of scintillation study. The results show that peak TEC values were recorded during the months of October–November, and the lowest values during the months of July–August. The diurnal peak of TEC occurs between 10:00 and 14:00 UT hours. Seasonally, the ascending and descending phases of TEC were observed during the equinoxes (March and September) and solstice (June and December), respectively. The scintillations observed during the study were classified as weak ($0.1 \leq S4, \sigma_\Phi \leq 0.3$) and strong ($0.3 < S4, \sigma_\Phi \leq 1.0$). The diurnal scintillation pattern showed peaks between 17:00 and 22:00 UT hour, while the seasonal pattern follows the TEC pattern mentioned above. Amplitude scintillation was more dominant than phase scintillation during the two years of the study. Scintillation peaks occur during the months of March–April and September–October, while the least scintillations occur during the months of June–July. Therefore, the contribution of this study is filling the gap in the current documentation of amplitude scintillation without phase scintillation over the Ugandan region. The scintillations observed have been attributed to wave-like structures which have periods of about 2–3 h, in the range of **that of large scale travelling ionospheric disturbances (LSTIDs)**.

Keywords: Low latitude scintillation; Scintillation and TEC climatoloty; Ionospheric irregularities

1. Introduction

Plasma distortions during perturbed ionospheric conditions have become detrimental to the technologically advancing world. Turbulence in the ionosphere leads to development of ionospheric irregularities. These irregularities manifest as enhancements or depletions of the electron density embedded in the ambient ionosphere, and may last for minutes to a few hours. The presence of moving irregularities in the ionosphere causes fluctuations in signal intensity, phase, polarisation, and angle of arrival. Rapid random and temporal fluctuations of signal intensity and

* Corresponding author at: Department of Physics, Mbarara University of Science and Technology, Mbarara, Uganda. Tel.: +256 702214144; fax: +256 454436514.
E-mail addresses: emirant.amabayo@gmail.com (E.B. Amabayo), ejurua@gmail.com (J. Edward), pjcilliers@sansa.org.za (P.J. Cilliers), jhabarulema@sansa.org.za (J.B. Habarulema).

[1] Tel.: +256 712 638268; fax: +256 485 20782.
[2] Tel.: +27 (28) 312 1196; fax: +27 (28) 312 2039.

0273-1177/$36.00 © 2014 COSPAR. Published by Elsevier Ltd. All rights reserved.
http://dx.doi.org/10.1016/j.asr.2013.12.015

phase referred to as amplitude and phase scintillations respectively, predominantly occur in the F layer. This phenomena is particularly severe in the tropical regions during evenings around the equinoxes and in the auroral zones. Ionospheric scintillation is a function of solar activity, geomagnetic activity, time of the year, local time, and geographic location. However, some facts about physical mechanisms responsible for scintillation occurrence remain difficult to understand, making it unpredictable. Despite significant attempts to understand the ionospheric behaviour, little knowledge exists about the climatology, distribution and morphology of scintillation phenomena over low latitude Africa. This is principally due to lack of instruments to provide a continuous database over the low latitude African region. This has often posed limitations on the attempts to forecast and nowcast scintillation occurrence on regional basis.

Ionospheric scintillation can be observed from the rapid variation in the received carrier-to-noise ratio ($\frac{C}{N_o}$) on GPS L-band signals and the frequency of occurence of cycle slips in the phase of the signal. The presence of reflecting obstacles in the vicinity of the receiving antenna can cause multipath effects, similar to scintillations associated with ionospheric irregularities (Romano et al., 2013). Multipath effects have been removed from this study by considering only scintillation events observed by satellites above 30° elevation. A GPS receiver's ability to cope with scintillation depends on the frequency of occurrence of scintillation, on the detection algorithm, as well as on the radio frequency and the position (azimuth, elevation) of the observed satellite (Conker et al., 2000). Frequent scintillation may not allow enough time for the GPS receiver to recover from cycle slips or loss of lock before the next scintillation causes loss of lock. Therefore, sufficiently intense signal fluctuations cause GPS receivers failure to track signals from GPS satellites during loss of lock, which may increase navigation errors or even cause navigation failure (Kintner et al., 2007). Radio communication systems are known to be seriously affected by ionospheric disturbances which in turn limit the ability of the receiver system to coherently integrate weak signals (Dierendonck et al., 1993). Current documentation shows that complete loss of GPS capability can result from scintillations, under certain conditions. This loss of information from some or all satellites causes a drawback to both civilian and military satellite navigation systems. Therefore, a low latitude scintillation study is very important for systems that rely upon GPS satellite observation. These include satellite-based communication and navigation systems, and also scientific instruments requiring observations of trans-ionospheric radio signals (e.g., radio-astronomy). Recent study conducted by Habarulema et al. (2013) over the African equatorial latitudes revealed positive storm effects during the main phase of the storm and negative storm effects over both mid and equatorial latitudes during the recovery phase. The authors observed a shift in the equatorial TEC enhancement from one station to another during the storm period, attributed to the passage of TIDs (Adewale et al., 2008). TIDs are generally a manifestation of atmospheric gravity waves (GWs) in the ionosphere (Alfonsi et al., 2013).

According to Kintner et al. (2007), ionospheric scintillation occurs mostly at the low and high latitudes with a much lower incidence in mid-latitudes. Low latitude ionospheric irregularities have been attributed to decreased ionospheric conductivities as a result of plasma bubbles, plasma drifts, neutral winds and pre-reversal enhancement of the equatorial eastward electric field (Du et al., 2000). However, equatorial scintillation has been attributed mainly to the ionospheric equatorial anomaly (Dubey et al., 2005), which in turn is associated with the sharp electron density gradients within such a region. In terms of geomagnetic distribution, ionospheric scintillation generally peaks in the sub-equatorial anomaly regions, located approximately ± (10°–20°) north or south of the magnetic equator. Based on in situ and ground-based measurements, Wernik et al. (2004) observed that ionospheric irregularities are concentrated near the magnetic equator and are observable during the pre-midnight period. According to Li et al. (2006), scintillation observed at low latitudes are primarily controlled by the generation and growth of irregularities over the magnetic equator. This is where the effects of upward plasma ($E \times B$) drift and effective ion recombination at lower altitudes result in a steep gradient of electron density on the bottomside F region. When the altitude of the F region is high enough or the bottomside background electron density gradients are large enough to overcome recombination effects, the RayleighTaylor (R–T) instability mechanism initiates a growth in plasma fluctuations. The nearly horizontal magnetic field at low latitudes provides a conducive environment for the generation of irregularities by the generalised R–T instability (GRT) mechanism. This mechanism occurs very frequently in the post-sunset equatorial ionosphere, resulting in the explosive release of the stored gravitational energy in the ionosphere. Irregularities of different scale sizes (ranging from centimetres to kilometres) develop and create an intense scintillation environment (Adewale et al., 2012), leading to communication and navigational problems (Alfonsi et al., 2013; Cabrera et al., 2010; Abdu, 2001).

According to Abdu (2001), the growth of R–T instability responsible for equatorial ionospheric irregularities is summarised by the exponential growth profile in Eq. 1.

$$A = A_o e^{\gamma t}, \tag{1}$$

where A_o is the initial instability and t is the time of instability growth. The growth rate γ in Eq. 1 can be expanded to give a GRT instability growth rate when chemical recombination is neglected as in Eq. 2.

$$\gamma \approx \underbrace{\frac{\Sigma_P^F}{\Sigma_P^E + \Sigma_P^F}}_{a}\left[\underbrace{\frac{E \times B}{B^2}}_{b} + \underbrace{U_n}_{c} + \underbrace{\frac{g}{\nu^{eff}}}_{d}\right]\underbrace{\frac{\partial N}{N \partial h}}_{e}, \tag{2}$$

where Σ_P^F and Σ_P^E are the contributions to the flux-tube integrated Pedersen conductivity from the E and F regions, respectively, h is the height above the earth, v^{eff} is the effective ion and neutral collision frequency, U_n is the neutral wind velocity component perpendicular to the magnetic field and g is the gravitational acceleration. Martins et al. (2005) pointed out that the post-sunset enabling effects occur when term a approaches unity, which consequently increases term e. The upward post-sunset $E \times B$ drifts (term b) are believed to be the main driving mechanisms for generation of equatorial ionospheric irregularities. The greatest growth rate (i.e., enhancing effect) occurs when the peak height of the ionosphere is high (i.e., when the ionosphere moves to high altitudes). This reduces the neutral and ion collision frequency, which in turn maximises term d when the bottomside density gradient is sharp. The gravitational force on the electrons and ions causes them to drift parallel to the boundary. The $E \times B$ drift produced in the opposite direction amplifies the initial perturbation. When such a disturbance moves onto the surface of the interface in the form of a wave (GWs) are generated and these in turn provide a seed mechanism for the R–T instability (Huang et al., 2002; Hoang et al., 2010; Balthazor and Moffett, 1997). When GWs propagate perpendicularly to the magnetic field, they generate polarised electric fields, and these are amplified non-linearly by the R–T instability (Huang et al., 2002; Cabrera et al., 2010). The positive electron density gradient region of the rapidly rising F layer bottomside becomes unstable due to density perturbations. This leads to the growth of plasma bubble irregularities by the R–T instability mechanism. The plasma bubbles develop as flux tubes aligned vertically. The secondary irregularities develop by cascading processes at the steepening density gradients of the bubbles along side the large rising plasma depletions (Abdu, 2001). The vertical plasma drift and the subsequent increase in the evening F layer height are due to the pre-reversal electric field enhancement. The pre-reversal electric field is controlled by the thermospheric zonal wind (eastward in the evening) and by the longitudinal gradient in the integrated E region conductivity near sunset time. The electron density in the lower ionosphere rapidly decays at night (due to absence of sunlight) and a steep vertical density gradient develops on the bottomside of the raised F layer. A density perturbation under certain conditions can trigger the R–T instability on the bottomside of the F layer. The instability in turn initiates development of plasma irregularities and field aligned depletions which then drift upwards through the F layer.

The scintillation data used in this study was obtained from the SCINDA installed at Makerere University, Uganda. While the TEC data is archived by two dual frequency recievers installed at Mbarara and Entebbe, both in Uganda. The details of the receiver stations and their data sampling intervals are provided for in Table 1. This study provides information on both amplitude and phase scintillation characteristics. The current literature on scintillation over Ugandan region mainly deals with amplitude scintillation and does not cater for phase scintillation characteristics. Therefore, this current study aims at establishing the climatology of ionospheric scintillation and TEC over the Ugandan region. The study will then offer basis for developing a regional based scintillation or TEC model.

2. Data description and analysis

Amplitude scintillation is quantified by the S4 index, which is essentially a normalised standard deviation of the signal intensity measured at 50 samples per second over a time period (Datta-Barua et al., 2003) of typically 1 min and is expressed as

$$S_4 = \sqrt{\frac{\langle I^2 \rangle - \langle I \rangle^2}{\langle I \rangle^2}} \tag{3}$$

where I is the mean incoming signal power in watts (W). Severe amplitude scintillation reduces the $\frac{C}{N_o}$ at the GPS receiver and this causes the received signal intensity to drop below the receiver's lock threshold. This forces the receiver to re-acquire the signal and leads to errors in both GPS carrier measurements and GPS code (or loss of code lock). The lock threshold is determined by the bandwidth of the GPS receiver system and depends on the receiver tracking channel.

Phase scintillation is known to complicate cycle slip detection and measurement since it can affect cycles of L_1 or L_2 signals between two epochs with a common epoch rate of $\leqslant$10 s (Wanninger, 1993). Phase variations are often quantified in terms of the sigma phi index (σ_ϕ) which is the standard deviation of the refractive component of the GPS

Table 1
Geophysical parameters of the GPS stations.

Station	Station ID	Geographic coordinates		Geomagnetic coordinates		Resolution (s)
		long (°E)	lat (°N)	long (°E)	lat (°S)	
IGS						
Mbarara	MBAR	30.74	−0.60	102.91	2.82	30
Entebbe	EBBE	32.44	0.04	104.70	2.47	15
Mt. Baker	BAKC	29.89	0.35	102.23	1.75	15
SCINDA						
Makerere	MAK	32.57	0.34	104.87	2.20	30
Mbarara	MBAR	30.66	−0.62	102.83	2.82	30

signal phase deviation produced during transit through the ionosphere. It is expressed as follows

$$\sigma_\phi = \sqrt{\langle \phi^2 \rangle - \langle \phi \rangle^2} \quad (4)$$

where ϕ is the signal phase in degrees or radians, and <> indicates averaging over a period of 1 min. Phase scintillation can cause GPS receiver systems to lose lock on the signal due to rapid changes in the signal frequency. The apparent range rate errors can produce a Doppler shift change in GPS signals. When the shift exceeds the bandwidth of the phase lock loop (PLL), it results in loss of phase lock.

A custom MATLAB algorithm developed at SANSA was used in processing scintillation data. This software was first implemented by Adewale et al. (2012) and it was modified for this study. This algorithm uses a custom programme called "**parseismr.exe**" to extract the parameters of interest from the binary files. Filtering of data is done by defining scintillation and elevation thresholds. Low and high level S4 and σ_ϕ thresholds of 0.05 and 1.2, respectively were set to remove outliers. Scintillation events below 20° elevation were filtered out (or removed). Scintillation events associated with anomalous PRN (pseudo-random number) values (Geostationary Satellite Data) were removed. The monthly percentage occurrence (i.e., probability) were computed using the following formula:

$$\text{Probability} = \frac{\text{Sum of actual observations}}{\text{Total number of observations expected}} \times 100\% \quad (5)$$

Monthly data availability was computed using a similar expression. Multi year plots and maps were produced for time binning of 10 min. The technique used to derive TEC along the signal path between the receiver and the GPS satellite, commonly referred to as slant TEC (*STEC*)

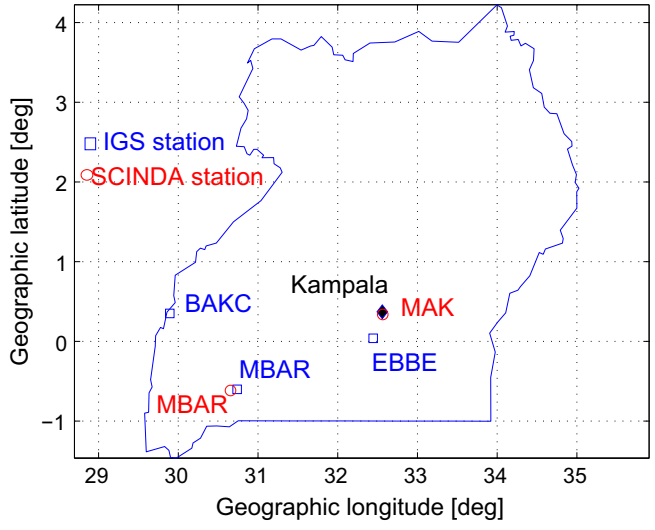

Fig. 1. Map of Uganda showing the IGS and SCINDA GPS receiver infrastructure.

is well documented in Amabayo et al. (2012) and Hoffmann-Wellenhof et al. (1992). The current GPS network over Uganda consists of two SCINDA receivers and three IGS receivers. The two SCINDA receivers (i.e., the last two in the Table 1) are installed at Makerere University (MAK, 0.34°N, 32.57°E) and Mbarara University (MBAR, 0.62°S, 30.66°E). The scintillation data at Mbarara was ignored in this study due to too many data gaps. Fig. 1 shows the geographical locations of the GPS receivers. **The current study investigated the diurnal, monthly and seasonal variability of TEC, σ_Φ and S4 scintillation indices over Ugandan region for two years (2011 and 2012). The study classified the scintillation events observed as weak ($0.1 \leqslant S4, \sigma_\Phi \leqslant 0.3$) and strong ($0.3 < S4, \sigma_\Phi \leqslant 1.0$). The IGS receiver at Mt. Baker (BAKC) only has data from 2008–06-15 to 2011–08-15 and hence was excluded in this study.**

3. Results and discussion

The results presented in this paper are based on the diurnal, seasonal and annual variations of S4, σ_Φ and vertical TEC (VTEC). A number of studies such as Ngwira et al. (2013), Oron et al. (2013) and Dujanga et al. (2013) have presented amplitude scintillation and TEC measurements without phase scintillation over Ugandan region. The contribution of this study is the derivation of phase scintillation from SCINDA files with the extension *.ism. This study therefore extends the understanding of the scintillation phenomena over the Ugandan region. Careful analysis of scintillation data has shown that both strong and weak amplitude and phase scintillation occurs over Ugandan region. In this study, amplitude and phase scintillation either occurs independently or simultaneously. This study considered scintillation events with S4 and σ_Φ index above 0.1 as significant. The scintillation events were further analysed to obtain their characteristics as a function of time and season. Figs. 2(a)–(f) show that high scintillation levels ($S4, \sigma_\Phi \geqslant 0.4$) were observed during the two year study. The low latitude ionospheric scintillations observed in this study occur mostly between post local sunset and midnight. Most of the scintillation events observed occur between 17:00 and 22:00 UT hours (Ugandan standard time (UST) = UT hr + 3 h). It was observed that simultaneous occurrence of amplitude and phase scintillations dominate the statistics. There were also cases where the two occur separately as shown in Fig. 2(g). These plots show that Makerere SCINDA receiver recorded meaningful scintillation events ($S4 \geqslant 0.4$). The scintillation occurrence intensifies between 18:00 and 22:00 UT hours. Selected PRN scintillation data for the selected days was analysed and the results are shown in Figs. 3.

Figs. 3 show that on selected days, strong scintillation levels ($S4, \sigma_\Phi \geqslant 0.4$) were observed between 18:30 and 20:30 UT hours along the ray paths to PRNs 15, 6 and 11. Weak phase scintillation ($0.1 \leqslant \sigma_\Phi \leqslant 0.3$) was observed along the ray path to PRN 30, while strong

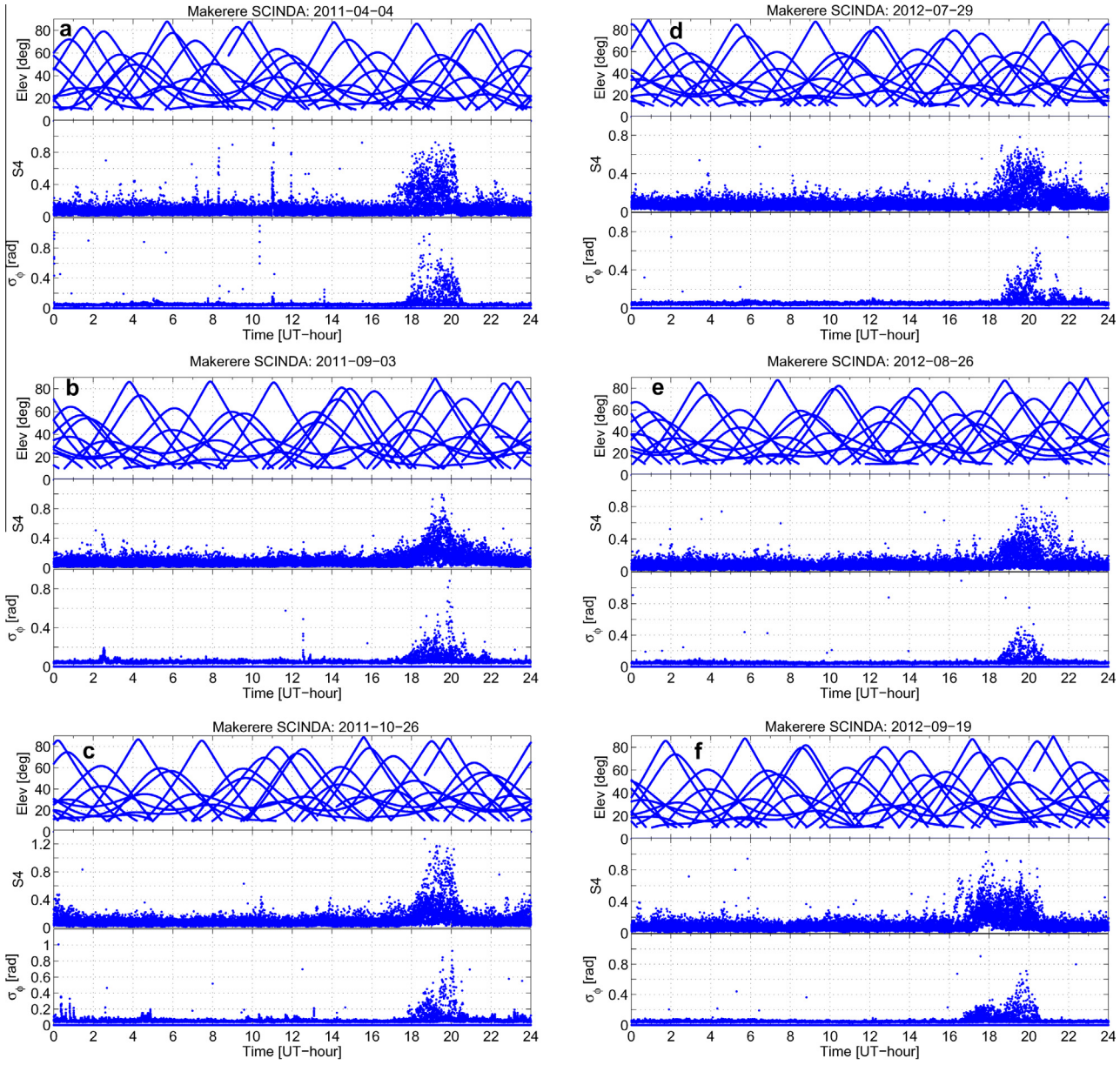

Fig. 2. Sample plots of elevation angle, S4-index, σ_Φ superimposed for selected days of 2011 (a)–(c) and 2012 (d)–(f) and amplitude without phase scintillation (g).

S4 levels were observed on 2012–07-29. Along the ray paths to PRNs 3 and 19, strong S4 and weak σ_Φ levels were observed between 17:00 and 21:00 UT hours on 2012–08-26 and 2012–09-19. The $\frac{C}{No}$ pattern remained normal throughout these events, except on PRN 11 at $\sim$ 19:00 UT on 2011–10-26 where a slight decrease was observed. Scintillations above 30° along the ray paths to these satellites was considered significant, otherwise any event below 30° is considered to be multipath effect. A study by Alfonsi et al. (2011), associated the narrow band of amplitude and phase scintillation at low latitudes with small values of $\langle ROT \rangle$. Our study found out that the variation of ROT during the events observed range from 1 to 4 TECU at all levels of scintillation. Continuos wave transform (with morlet as a mother wavelet) was carried out on TEC data for selected PRNs. During the wavelet analysis, ΔTEC which is computed by subtracting fourth order fitted polynomial values from actual TEC data, was used. A fourth order polynomial function is fitted to TEC data (for selected PRNs) to remove diurnal TEC pattern and reveal TEC perturbations. The Morlet wavelet was used because of its shape's similarity to geophysical parameter (Torrence and Compo, 1998; Chane-Ming et al., 2000; Habarulema et al., 2013). This was primarily aimed at attempting to trace the driving mechanisms behind the night-time scintillations observed. Wavelet analysis was performed on ΔTEC to extract dominant wave modes in time series

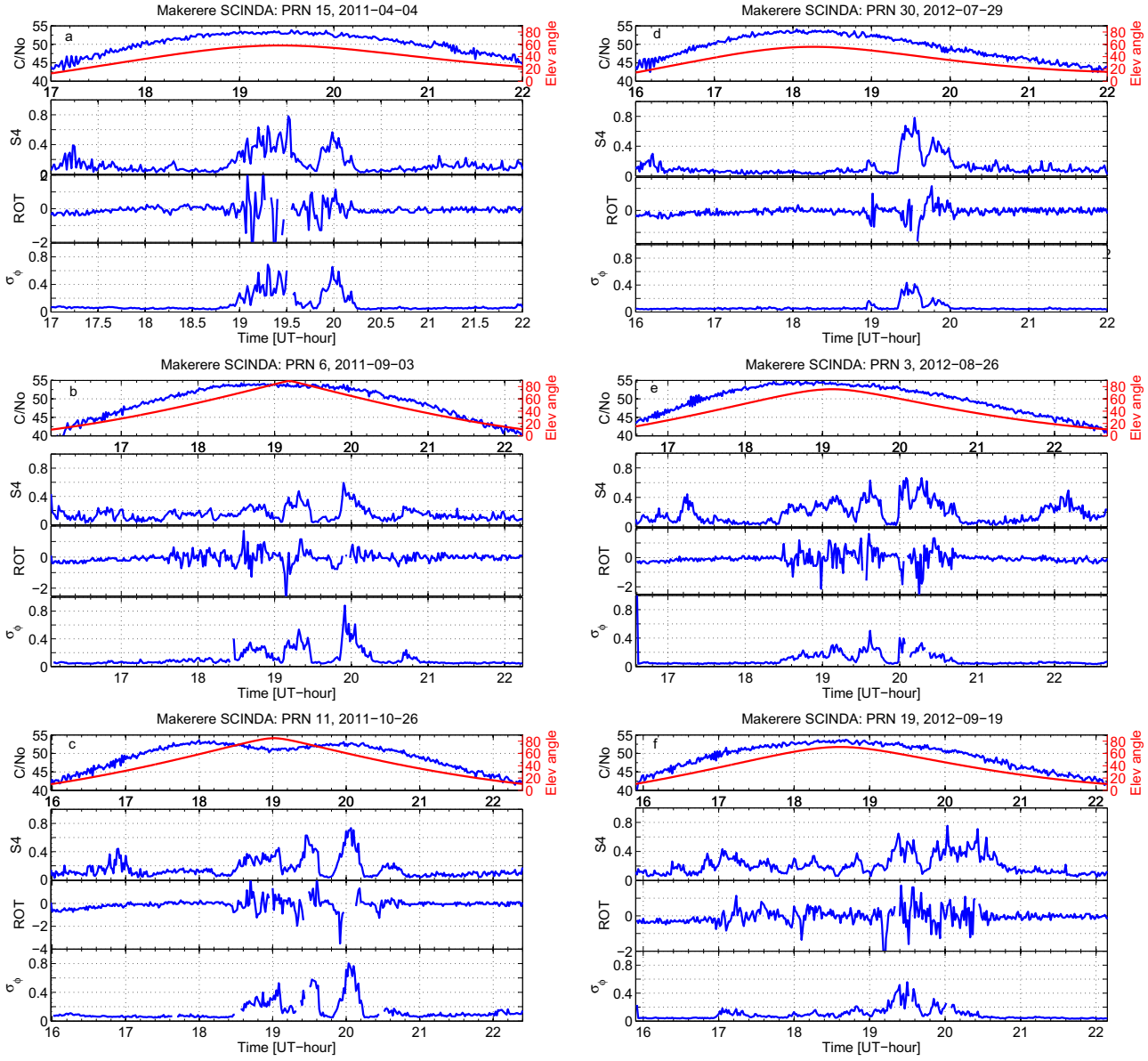

Fig. 3. Showing L1 $\frac{C}{No}$ (dB), elevation angle, S4 index, ROT (TECU/min) and σ_Φ for selected satellites on the above days of 2011 (a)–(c) and 2012 (d)–(f).

data. The analysis was done by using different periods at Entebbe and Mbarara IGS stations to ensure that there is no overlap in observations (in terms of GPS coverage). **Wave-like structures with period ranging from 2–3 h were observed between 17:00 and 20:00 UT along the ray paths to PRN 11 as shown in Fig. 4(a). Similar structures with periods 2–3 h were also observed between 17:00 and 22:00 UT along the ray paths to PRNs 3 (Fig. 4(a)) and 30 (Fig. 4(b)). Wave-like structures with periods between 3 and 4 h were observed along the ray paths to PRNs 15 (Fig. 4(a)) and 19 (Fig. 4(b))**. This shows a statistical representation of wave-like structureswhich have periods in the range of TIDs. The interaction between thermospheric GWs and the ionosphere has been known to generate Travelling Atmospheric Disturbances (TADs) which manifest as TIDs either of medium scale or large scale (Huang et al., 2002; Hoang et al., 2010; Balthazor and Moffett, 1997). The periods of the wave-like structures observed in this study are consistent with those detected by Habarulema et al. (2013). These wave-like structures are observed during the same period with high scintillation events and so TIDs could be the associate causes of the scintillations observed (Borries et al., 2010; Yuan et al., 2009). These wave-like structures are associated with large scale TIDs with horizontal scale size >1000 km (Ding et al., 2008; Davies, 1990). According to Wanninger (1993) these structures are believed to have horizontal phase speeds and periods ranging from about 300 m/s to 1000 m/s and ~30 min to ~3 h, respectively.

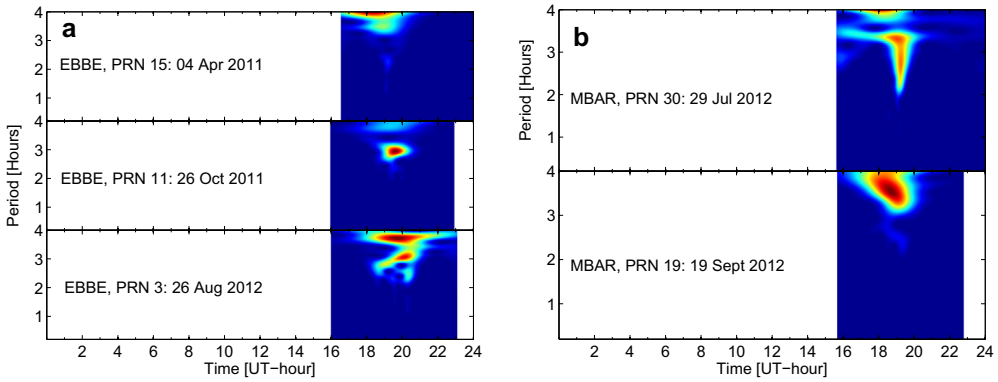

Fig. 4. Wavelet transforms of diurnal TEC over EBBE (a) and MBAR, (b) stations for selected PRNs.

3.1. Scintillation statistics and climatology

This section provides a description of the statistics and climatology of scintillation phenomena over Uganda for events above 30° elevation. Fig. 5 gives the statistics of data availability and classification of the observed scintillation. The morphology of scintillation has been described in terms of percentage occurrence in specified threshold level of S4 and σ_Φ index. The study is made in terms of hourly and monthly variations of S4 and σ_Φ index observed in GPS signals at Makerere.

Fig. 5(a) shows that a small percentage of data was available in January (25%) and November (40%) in 2011. Data availability was very low in the months of June (16%) and November (1.81%) in 2012. The presence of data gaps in 2012 has affected the characterisation of ionospheric scintillation observed over Uganda. It can be observed from Fig. 5(b) that occurrence of both amplitude and phase scintillation dominates the occurrence of strong scintillation, with peak occurrence of 4.8% in November, 2011. The peak occurrence in 2012 is at 2.29% in September, lower than the second peak occurrence of 2.40% in April, 2011. Fig. 5(b) shows that 1.79% peak occurrence of strong amplitude scintillation was registered in June, 2012, accompanied by very low occurrence of strong phase scintillation. Weak scintillation occurrence in Fig. 5(c) is dominated by 3.81% occurrence of both amplitude and phase scintillation in January, 2011. This was followed closely by 3.26% peak occurrence of weak amplitude scintillation in January, 2011. Low occurrence of weak phase scintillation were registered with a lower peak (1.79%) during June solstice of 2012 (Li et al., 2011). These results are in good agreement with the results of similar work done by Spogli et al. (2013) and Deng et al. (2013) among others. Similar study by Adewale et al. (2012) revealed that scintillation diurnal and seasonal percentage occurrence shows peaks during the equinox months (March and April) at 23:00 local time.

3.2. Diurnal and seasonal variation of scintillation

Amplitude and phase scintillation maps were created for the SCINDA receiver at Makerere using the available two year data. These maps were obtained by considering 10 min bins of the mean scintillation indices. The general trend showed by the maps indicate that average S4 (Fig. 6(a) and (b)) and σ_Φ (Fig. 6(c) and (d)) values did not exceed 0.8. The smallest values were observed during June solstice of 2011, while no data for this month in 2012 as recorded from Makerere (Fig. 6(b) and (d)). The average peak S4 values are observed from 17:00 to 22:00 UT hours and range from 0.4 to 0.7 in the months of

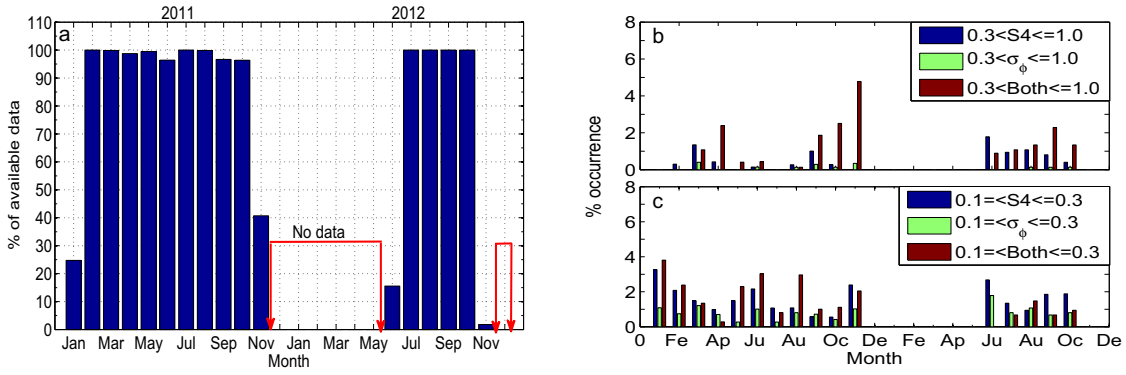

Fig. 5. Showing (a) percentage of available data, percentage occurrence of, (b) strong and (c) weak amplitude and phase scintillation observed from Makerere in 2011 and 2012.

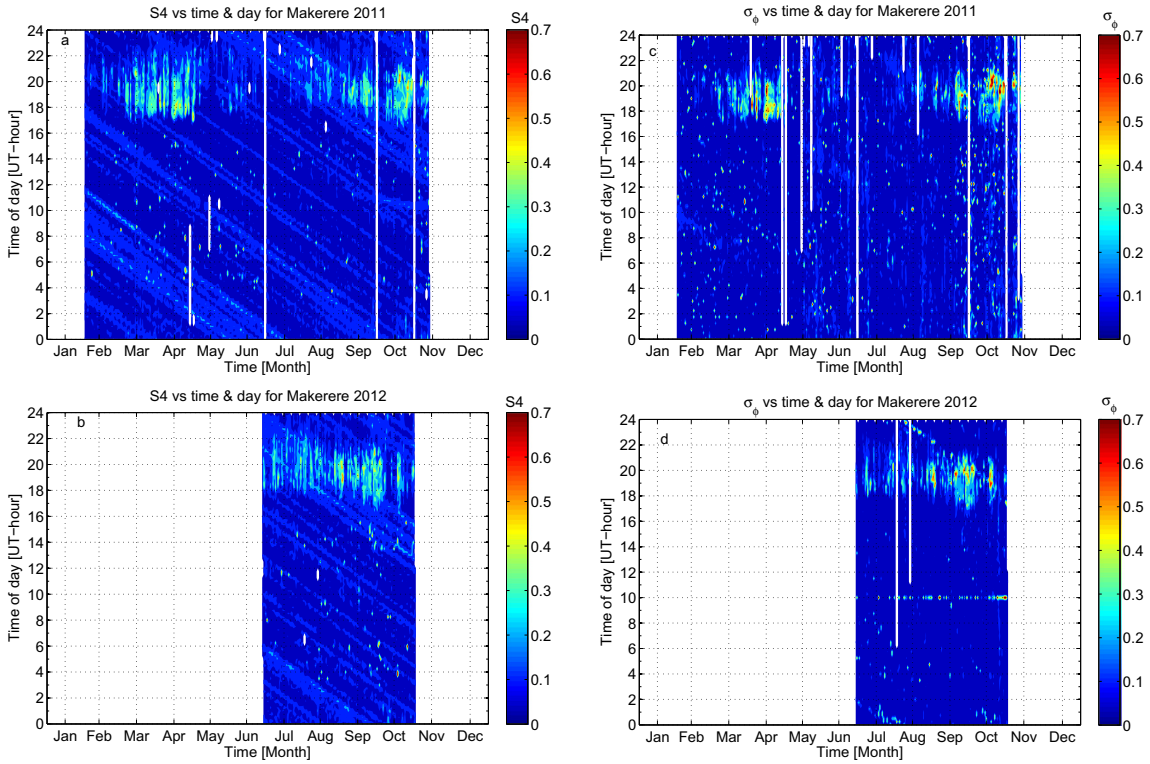

Fig. 6. Scintillation maps for amplitude (a, b) and phase (c, d) scintillation showing the diurnal and seasonal variation for Makerere SCINDA station.

March–April and September–October. This general pattern confirms that the significant scintillation events were recorded during the period of study, despite data gaps. A recent amplitude scintillation study over Kenya at VHF and L-band frequencies revealed peak occurrence during the post-sunset hours of the equinoctial months than at the solstice and after midnight. The detailed description of the results of the study can be found in Olwendo et al. (2013). This particular study adds the statistical characteristics of phase scintillation, the first of its kind over the region. This study also shows that amplitude and phase scintillation mostly occur simultaneously over the region. Paznukhov et al. (2012) used automated technique of spectral analysis to extract and identify equatorial plasma bubbles (EPBs) from the GPS TEC measurements. They concluded that the seasonal climatology of the EPBs and GPS scintillations in equatorial Africa can be adequately explained by the alignment of the solar terminator and local geomagnetic field. The post-sunset peaks observed in this current study are most likely associated with low latitude **wave-like structures observed in Fig. 4. The daytime equatorial eastward dynamo electric fields generated in the *E* region by thermospheric winds often diffuse along the magnetic field lines to the F-region altitudes. These electric fields cause upward (E×B) drift of the plasma during the daytime. Near sunset, plasma densities and dynamo electric fields in the *E* region decrease, and at this local time another dynamo develops in the *F* region. A combination of polarisation charges within conductivity gradients across the terminator and the increased eastward neutral wind component enhances the eastward electric field. The post-sunset electric field causes upward drift of ionospheric plasma, and eventually the electric field turns westward, causing plasma to drift downward. Consequently after sunset, vertical plasma density gradients form in the bottomside of the *F* layer. The upward density gradient is opposite in direction to the gravitational force. This configuration becomes Rayleigh–Taylor (R–T) unstable and allows plasma density irregularities to form (Alfonsi et al., 2013) [references here in]. Gravity waves from the troposphere are important source of energy transfer in the ionosphere-thermosphere system (Cabrera et al., 2010) and hence responsible for the post-sunset uplift of plasma. Therefore, the post-sunset peaks observed in this study are most likely associated with low latitude wave-like structures in Fig. 4(a) and (b).**

3.3. TEC variability

The *F* region plasma density significantly contributes to the diurnal TEC variability. Current documentation shows that increase (enhancement) or decrease (depletion) of TEC values are well correlated with scintillations in the *F* region (Deng et al., 2013; Oron et al., 2013; Dujanga et al., 2013). Small-scale irregularities often associated with TEC depletions are responsible for the strong scintillations observed. TEC maps were developed for the two years of this study for the receivers at EBBE Fig. 7(a) and Mbarara Fig. 7(b). The corresponding *n*-degree polynomial fit is also provide in Figs. 7(c) and (d). Fig. 7 displays the diurnal pattern of the TEC observed from EBBE (a) and MBAR

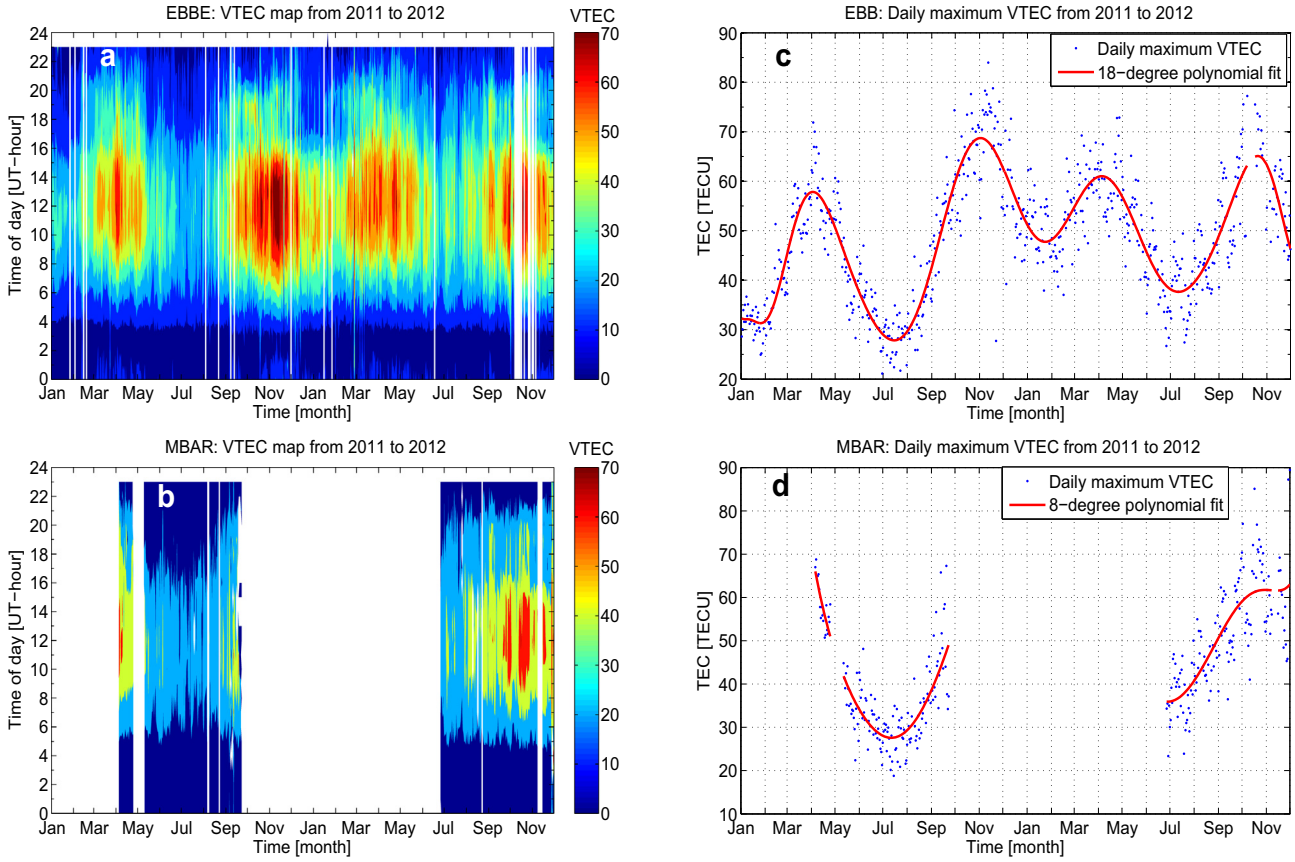

Fig. 7. TEC maps showing diurnal and seasonal variation of daily maximum (a, b) and a polynomial fit (c, d) to the TEC data. The white spaces in the maps indicate absence of data.

(b) IGS stations for the different months of 2011 and 2012. This figure shows that TEC achieves a maxima during the months of April and November, while its minima occurs during January and July throughout the study period. The seasonal pattern shows that ascending and descending phases of TEC occur during equinoxes (March and September) and solstices (June and December). These observations can be viewed clearly from the *n*-degree polynomial fits, despite the overwhelming gaps in Mbarara data. It is important to note that the algorithm used determines the degree of the fit automatically depending on the data supplied. The lower value of the degree of fit for MBAR station VTEC may be attributed to the data outages. At the same time, the diurnal variability of TEC during these months is that it increases from 6:00 UT and shows a peak at 12:00 UT and decreases down up to 22:00 UT. This pattern is a signature of the variability of solar radiation and zenith angle at low latitudes.

4. Conclusion

This is the first study to investigate the statistical features of simultaneous observation of amplitude and phase GPS L-band scintillations over Ugandan region. The study is an overview of the statistical characteristics of the low latitude scintillations and the associated TEC variability based on the data collected with GPS receivers. The results show the occurrence frequency of post-sunset scintillation observed mainly between 17:00 to 22:00 UT hours. The seasonal TEC pattern shows peaks just after the equinoxial months. The minimum of the seasonal scintillation pattern occurs in the months of January, June and July. The results of this particular study are consistent with similar works done in other low latitude regions by Spogli et al. (2013) and Deng et al. (2013)) among others. This study has added the phase scintillation statistics to those reported by Ngwira et al. (2013), Oron et al. (2013) and Dujanga et al. (2013) and others over Ugandan region.

Acknowledgement

The authors acknowledge the International Science Program (ISP) for funding this study and Mr. Joseph Olwendo for his contribution towards the software used in data analysis. The effort made by Dr. Anguma Simon Katrini towards this study is also acknowledged by the authors. We extent our appreciation to the Boston College and the Air Force Research Laboratory (AFRL), USA, for supplying the SCINDA receiver at Makerere University. IGS data used in this study was downloaded from ftp://data-out.unavco.org/pub/rinex/obs. The authors greatly thank and acknowledge the corrected cited by the reviewers to improve the quality of this paper.

References

Abdu, M.A., 2001. Outstanding problems in the equatorial ionosphere-thermosphere electrodynamics relevant to spread F. J. Atmos. Solar-Terr. Phys. 63, 869–884.

Adewale, A.O., Oyeyemi, E.O., Adeloye, A.B., Mitchell, C.N., Rose, J.A.R., Cilliers, P.J., 2012. A study of L-band scintillations and total electron content at an equatorial station, Lagos, Nigeria. Radio Sci. 47, RS2011. http://dx.doi.org/10.1029/2011RS004846.

Adewale, A.O., Oyeyemi, E.O., Adeloye, A.B., Ngwira, C.M., Athieno, R., 2008. Responses of equatorial *F* region to different geomagnetic storms observed by GPS in the African sector. J. Geophys. Res. 116, A12319. http://dx.doi.org/10.1029/2011JA016998.

Alfonsi, L., Spogli, L., Pezzopane, M., Romano, V., Zuccheretti, E., Franceschi, G.D., Cabrera, M.A., Ezquer, R.G., 2013. Comparative analysis of spread-F signature and GPS scintillation occurrences at Tucumàn, Argentina. J. Geophys. Res. Space Sci. 118, 4483–4502. http://dx.doi.org/10.1002/jgra.50378.

Alfonsi, L., Spogli, L., Tong, J., Franceschi, G.D., Romano, V., Bourdillon, A., Huy, M.L., Mitchell, C., 2011. GPS scintillation and TEC gradients at equatorial latitudes in April 2006. Adv. Space Res. 47, 1750–1757.

Amabayo, E., McKinnell, L.A., Cilliers, P., 2012. Ionospheric response over South Africa to the geomagnetic storm of 11–13 April 2001. J. Atmos. Solar-Terr. Phys. 8485, 6274.

Balthazor, R.L., Moffett, R.J., 1997. A study of atmospheric gravity waves and travelling ionospheric disturbances at equatorial latitudes. Ann. Geophys. 15, 1048–1056.

Borries, C., Jakowski, N., Jacobi, C., 2010. Observation of large scale waves in the thermosphere–ionosphere system. In: WPP-303 Proceedings for ESAs 2nd SWARM International Science Meeting.

Cabrera, M.A., Pezzopane, M., Zuccheretti, E., Ezquer, R.G., 2010. Satellite traces, range spread *F* occurrence, and gravity wave propagation at the southern anomaly crest. Ann. Geophys. 28, 1133–1140. http://dx.doi.org/10.5194/angeo-28-1133-2010.

Chane-Ming, F., Molinaro, F., Leveau, J., Keckhut, P., Hauchecorne, A., 2000. Analysis of gravity waves in the tropical middle atmosphere over La Reunion Island (21°S, 55°E) with lidar using wavelet techniques. Ann. Geophys. 18, 485–498.

Conker, R.S., El-Arini, M.B., Hegarty, C.J., 2000. Modeling the effects of ionospheric scintillation on GPS/SBAS availability.

Datta-Barua, S., Doherty, P.H., Delay, S.H., Dehel, T., Klobuchar, J.A., 2003. Ionospheric scintillation effects on single and dual frequency GPS positioning. In: Proceedings of ION GPS/GNNS 2003, Portland, OR, pp. 336–346.

Davies, K., 1990. Ionospheric Radio. Peter Peregrinus, London.

Deng, B., Huang, J., Liu, W., Xu, J., Huang, L., 2013. GPS scintillation and TEC depletion near the northern crest of equatorial anomaly over South China. Adv. Space Res. 51, 356–365.

Dierendonck, A.J.V., Klobuchar, J., Hua, Q., 1993. Ionospheric scintillation monitoring using commercial single frequency C/A code receivers. In: Proceedings of ION GPS-93, Institute of Navigation, Salt Lake City, UT.

Ding, F., Wan, W., Liu, L., Afraimovich, E.L., Voeykov, S.V., Perevalova, N.P., 2008. A statistical study of large-scale traveling ionospheric disturbances observed by GPS TEC during major magnetic storms over the years 2003–2005. J. Geophys. Res. 113, A00A01. http://dx.doi.org/10.1029/2008JA013037.

Du, J., Wilkinson, P., Thomas, R., Cervera, M., 2000. Determination of Equatorial Ionospheric Scintillation S4 Dual Frequency GPS 2000, URSI Commission G, Workshop, La Trobe University, Australia.

Dubey, S., Wahi, R., Gwal, A.K., 2005. Effects of ionospheric scintillation on GPS receiver at equatorial anomaly region Bhopal, URSI XXVII-Ith General Assembly, New Delhi, India, 01238.

Dujanga, F., Baki, P., Olwendo, J., Twinamasiko, B., 2013. Total electron content of the ionosphere at two stations in East Africa during the 24–25 October 2011 geomagnetic storm. Adv. Space Res. 51, 712–721.

Habarulema, J.B., McKinnell, L.A., Burešovà, D., Zhang, Y., Seemala, G., Ngwira, C., Chum, J., Opperman, B., 2013. A comparative study of TEC response for the African equatorial and mid-latitudes during storm conditions. J. Atmos. Solar-Terr. Phys. 102, 105–114.

Hoang, T.L., Abdu, M., MacDougall, J., Batista, I.S., 2010. Longitudinal differences in the equatorial spread *F* characteristics between Vietnam and Brazil. Adv. Space Res. 45, 351–360.

Hoffmann-Wellenhof, B., Lichtenegger, H., Collins, J., 1992. Global Positioning System Theory and Practice. Springer-Verlag, Wien New York.

Huang, C.Y., Burke, W.J., Machuzak, J.S., Gentile, L.C., Sultan, P.J., 2002. Equatorial plasma bubbles observed by DMSP satellites during a full solar cycle: toward a global climatology. J. Geophys. Res. 107 (A12). http://dx.doi.org/10.1029/2002JA009452.

Kintner, P., Ledvina, B.M., de Paula, E.R., 2007. GPS and ionospheric scintillation. Space Weather 5, S09003. http://dx.doi.org/10:1029/2006SW000260.

Li, G., Ning, B., Abdu, M.A., Yue, X., Liu, L., Wan, W., Hu, L., 2011. On the occurrence of postmidnight equatorial *F* region irregularities during the June solstice. J. Geophys. Res. 116, A04318. http://dx.doi.org/10.1029/2010JA016056.

Li, G., Ning, B., Wan, W., Zhao, B., 2006. Observations of GPS ionospheric scintillations over Wuhan during geomagnetic storms. Ann. Geophys. 24, 15811590.

Martins, C.R., Mendillo, M.J., Aarons, J., 2005. Toward a synthesis of equatorial spread *F* onset and suppression during geomagnetic storms. J. Geophys. Res. 110, A07306.

Ngwira, C.M., Seemala, G.K., Habarulema, J.B., 2013. Simultaneous observations of ionospheric irregularities in the African low-latitude region. J. Atmos. Solar-Terr. Phys. 97, 50–57.

Olwendo, O., Baluku, T., Baki, P., Cilliers, P., Mito, C., Doherty, P., 2013. Low latitude ionospheric scintillation and zonal irregularity drifts observed with GPS-SCINDA system and closely spaced VHF receivers in Kenya. Adv. Space Res. 51, 1715–1726.

Oron, S., Dujanga, F.M., Ssenyonga, T.J., 2013. Ionospheric TEC variations during the ascending solar activity phase at an equatorial station, Uganda. Indian J. Radio Space Phys. 42, 7–17.

Paznukhov, V.V., Carrano, C.S., Doherty, P.H., Groves, K.M., Caton, R.G., Valladares, C.E., Seemala, G.K., Bridgwood, C.T., Adeniyi, J., Amaeshi, L.L.N., Damtie, B., DUjanga, F.M., Ndeda, J.O.H., Baki, P., Obrou, O.K., Okere, B., Tsidu, G.M., 2012. Equatorial plasma bubbles and L-band scintillations in Africa during solar minimum. Ann. Geophys. 30, 675–682.

Romano, V., Spogli, L., Aquino, M., Dodson, A., Hancock, C., Forte, B., 2013. GNSS station characterisation for ionospheric scintillation applications. Adv. Space Res. http://dx.doi.org/10.1016/j.asr.2013.06.028.

Spogli, L., Alfonsi, L., Cilliers, P.J., Correia, E., Franceschi, G.D., Mitchell, C.N., Romano, V., Kinrade, J., Cabrera, M.A., 2013. GPS scintillations and total electron content climatology in the southern low, middle and high latitude regions. Ann. Geophys. 56, R0220. http://dx.doi.org/10.4401/ag-6240.

Torrence, C., Compo, G.P., 1998. A practical guide to wavelet analysis. Bull. Am. Meteorol. Soc. 79, 61–78.

Wanninger, L., 1993. Ionospheric monitoring using IGS data. In: Proceedings of the 1993 IGS Workshop, University of Berne, Berne, pp. 351–360.

Wernik, A.W., Lucilla, A., Materassi, M., 2004. Ionospheric irregularities, scintillation and its effects on systems. Acta Geophys. Pol. 52 (2), 237–249.

Yuan, Z., Ning, B., Deng, X., 2009. Effects of TADs on the *F* region of the mid-latitude ionosphere during an intense geomagnetic storm. Adv. Space Res. 44, 1013–1018.